Antibiotics

Towards Photochromic Azobenzene-Based Inhibitors for Tryptophan Synthase

Nadja A. Simeth[+],*[a, b] Thomas Kinateder[+],[c] Chitra Rajendran,[c] Julian Nazet,[c] Rainer Merkl,[c] Reinhard Sterner,[c] Burkhard König,[a] and Andrea C. Kneuttinger*[c]

Abstract: Light regulation of drug molecules has gained growing interest in biochemical and pharmacological research in recent years. In addition, a serious need for novel molecular targets of antibiotics has emerged presently. Herein, the development of a photocontrollable, azobenzene-based antibiotic precursor towards tryptophan synthase (TS), an essential metabolic multienzyme complex in bacteria, is presented. The compound exhibited moderately strong inhibition of TS in its *E* configuration and five times lower inhibition strength in its *Z* configuration. A combination of biochemical, crystallographic, and computational analyses was used to characterize the inhibition mode of this compound. Remarkably, binding of the inhibitor to a hitherto-unconsidered cavity results in an unproductive conformation of TS leading to noncompetitive inhibition of tryptophan production. In conclusion, we created a promising lead compound for combatting bacterial diseases, which targets an essential metabolic enzyme, and whose inhibition strength can be controlled with light.

Introduction

Antibiotics are crucial for modern medicine.[1] They are used to cure bacterial illnesses and infections, and to facilitate major surgical operations. Most of us have used them at least once in our lives. To further our understanding of their mode of action, antibiotic precursors are often designed for biochemical and pharmaceutical studies. This ultimately paves the way for drugs that are highly efficient, specific, and less prone to build-up of resistance. In particular, focusing on novel types of macromolecular targets and innovative strategies to circumvent resistance are paramount to this cause.[2]

Most antibiotics engage in bacterial cell-division processes or weaken the bacterial membrane.[3] Recently, the search for alternative targets was expanded to metabolic enzymes,[4] such as the well-investigated multienzyme complex tryptophan synthase (TS). TS catalyzes the last two steps of tryptophan biosynthesis in bacteria, plants, and fungi.[5] The complex consists of TrpA (α) and TrpB (β), which are arranged as a heterotetramer in a linear αββα configuration.[6] The functional unit of TS is thereby formed by one αβ heterodimer (Figure 1 A).[7] Tryptophan production starts with the TrpA reaction, in which indole-3-glycerol phosphate (IGP) is cleaved in a retro-aldol reaction to glyceraldehyde 3-phosphate (GAP) and indole.[7] In the next step, indole travels through an intermolecular channel to the active site of TrpB,[8] where it is used to synthesize tryptophan from serine by using pyridoxal phosphate (PLP) as a cofactor.[5b,9] Both reactions, indole synthesis in TrpA and tryptophan synthesis in TrpB, require tight allosteric regulation of both subunits (Figure 1 B).[6a,10] On binding of IGP in the TrpA active site, the affinity for serine in the TrpB active site is enhanced, as shown by a reduced K_M^{Ser} value, so that the initial reaction of serine with PLP to an aminoacrylate intermediate is facilitated.[8] The formation of the aminoacrylate in turn enhances the turnover of IGP to indole, as manifested in an increased k_{cat} value of TrpA.[11] Structural analysis of TS from *Salmonella typhimurium* revealed that a conformational change of the communication (COMM) domain, which includes around 90 residues in TrpB, is in particular responsible for the propagation of the allosteric signals between the two active sites.[12] In the absence of IGP and serine, the COMM domain exhibits an open conformation, while binding of IGP in TrpA and the subse-

[a] Dr. N. A. Simeth,[+] Prof. Dr. B. König
Institute for Organic Chemistry
Department of Chemistry and Pharmacy, University of Regensburg
Universitätsstrasse 31, 93040 Regensburg (Germany)
E-mail: n.a.simeth@rug.nl

[b] Dr. N. A. Simeth[+]
Stratingh Institute for Chemistry
Faculty of Science and Engineering, University of Groningen
Nijenborgh 4, 9747 AG Groningen (The Netherlands)

[c] T. Kinateder,[+] Dr. C. Rajendran, J. Nazet, Prof. Dr. R. Merkl,
Prof. Dr. R. Sterner, Dr. A. C. Kneuttinger
Institute for Biophysics and Physical Biochemistry
Regensburg Center for Biochemistry, University of Regensburg
Universitätsstrasse 31, 93040 Regensburg (Germany)
E-mail: andrea.kneuttinger@ur.de

[+] These authors contributed equally.

Supporting information and the ORCID identification numbers for the authors of this article can be found under: https://doi.org/10.1002/chem.202004061.

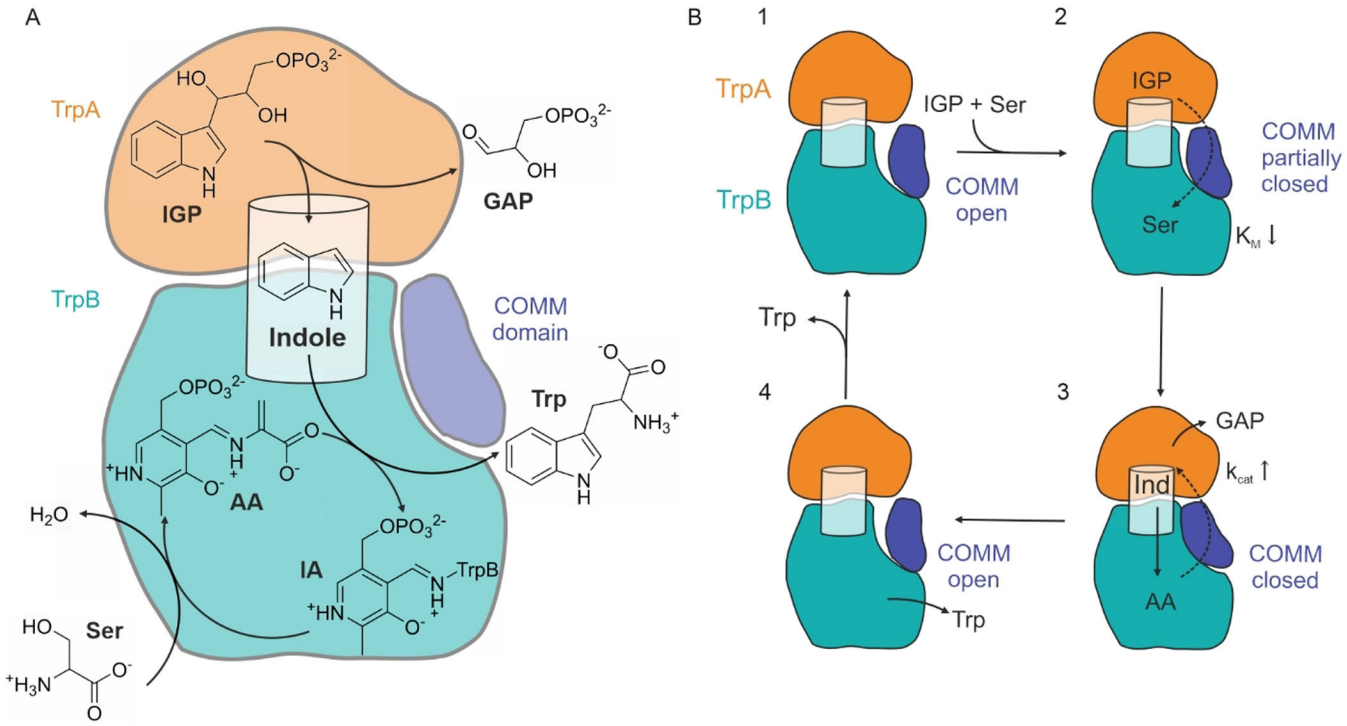

Figure 1. Schematic representation of the tryptophan synthase (TS) functional unit, its reactions, and allosteric regulation. A) In TrpA (orange) indole-3-glycerol phosphate (IGP) is cleaved into glyceraldehyde 3-phosphate (GAP) and indole, which is channeled through a hydrophobic tunnel (white) to TrpB (cyan). In TrpB, pyridoxal phosphate, bound as internal aldimine (IA), reacts with serine (Ser) to form aminoacrylate (AA), which subsequently reacts with indole to the final product tryptophan (Trp). The communication (COMM) domain of TrpB is shown in dark blue. B) In the absence of serine and IGP, TS is inactive and the COMM domain in TrpB adopts an open conformation (1). Binding of IGP to the TrpA active site leads to a partial closure of the COMM domain and an allosteric activation of TrpB enhancing the binding affinity (K_M↓) for its substrate serine (2). The formation of AA from PLP and serine in TrpB results in a fully closed COMM domain and an allosteric activation of TrpA, which increases the turnover of IGP to indole (Ind) and GAP (k_{cat}↑, 3). Finally, Trp, the reaction product of AA and Ind, dissociates from TrpB, and the COMM domain returns to its inactive open conformation (4).[13c]

quent formation of aminoacrylate in TrpB induce a stepwise transition to a closed conformation.[12b,13] As mammals lack the genes for the biosynthetic pathway of tryptophan, TS represents an excellent target for the development of new antibiotics. Previous studies already reported inhibitors towards TS that compete with IGP for the active site of TrpA,[14] bind at the TrpA:TrpB interface,[15] or interact with the hydrophobic intermolecular indole channel in TrpB.[16] These examples provide good starting points for the development of antibiotic agents.

Direct control of the efficacy of drugs is an innovative approach in biochemical and pharmacological studies, which is increasingly used to gain in depth knowledge of the mode of action. Temporally resolved activation allows one to unambiguously associate the observed effect to the drug. Most recently, the spatiotemporal control of drugs has been addressed by developing light-responsive, bioactive molecules in the growing field of photopharmacology.[17] Besides many other applications, such as photosensitive proteins,[18] DNA modulators,[19] kinase inhibitors,[20] and PROTAGs,[21] the first photocontrollable antibiotics have been developed.[22] The principle of photopharmacology is based on a seemingly simple strategy; the designed drug consists of moieties that convey a biological response, such as an inhibitory effect toward the target structure, and a photoresponsive part that facilitates a light-induced structural change. Thus, the drug is rendered effective in one configuration and ineffective in the other. Moreover, the different photoisomers can exhibit different pharmacokinetic and pharmacodynamic properties. A frequently used photoactuator is azobenzene, a molecule consisting of two aryl units connected by a diazo bond (N=N). On irradiation with light of a specific wavelength, the thermodynamically more stable *E* isomer can be converted to its corresponding *Z* form. This configurational change affects several properties of the molecule including its UV/Vis absorption spectrum, its steric demand, its polarity, and, if embedded in a suitable bioactive structure, its affinity towards, for example, enzymes. The metastable *Z* isomer can be converted back to the *E* form by irradiation with light of lower energy or thermally.[23]

In recent years, we have pioneered the control of metabolic multienzyme complexes with diverse photoresponsive tools.[24] In the present work, we explored photocontrollable inhibitors for the essential multienzyme complex TS of the enteric human pathogen *S. typhimurium*[25] as potential antibiotic structures. We designed and synthesized a small library of azobenzene-based compounds, investigated their photochemical behavior, and thoroughly studied their mode of inhibition towards TS. Finally, we substantiated these findings with crystallographic and computational methods and outline a mode of action for this potential drug precursor.

Results and Discussion

Design and molecular realization

Previous studies have described various target sites for inhibitors in the TS complex.[14b,c,15,16] We reasoned that targeting the TrpA active site is a good starting point for the design of a photocontrollable inhibitor. Hence, we analyzed the crystal structures of TS with IGP or the inhibitor indole-3-propanol phosphate bound to TrpA[6c,12a] to identify the most important ligand–enzyme interactions and steric requirements for binding to the active site (Figure S1.1 in the Supporting Information). Since both ligands form strong hydrogen bonds to residues in the active site with their phosphate motif and their NH moiety (Figure 2A), we integrated these two groups into our inhibitor design.

Consequently, our synthetic ligands consist of a phosphate motif to which an NH-containing amide moiety is attached through an alkyl linker (Figure 2B). To allow for reversible photoswitching, we extended the binding part of the molecule with an azobenzene photoswitch attached to the carbonyl group.[26] Finally, we varied the length of the alkyl or aryl linker to find an inhibitor that exhibits the optimal geometry to bind to the TrpA active site in one but not in the other photoisomer. Furthermore, we hypothesized that the *E* isomers would show stronger binding, whereas the increased steric demand in the *Z* isomers should lead to weaker binding. Following this assumption, the inhibitors in *E* should competitively displace IGP and inhibit the TrpA reaction, while the *Z* isomer should allow for IGP binding and turnover. As a result, due to the strong dependence of the TrpB reaction on binding of IGP to the TrpA active site, we would be able to simultaneously control IGP turnover in TrpA, and tryptophan production in TrpB with light (Figure 2C).

Synthesis

For the synthesis of a small library of azobenzene-based inhibitors as defined in our design (Figure 2B), we started from commercially available 4-carboxyazobenzene (**1**, Scheme 1). We converted the carboxylic acid, by treatment with $SOCl_2$, to the corresponding acyl chloride **2**, which was directly treated with differently functionalized amines to give **3a–f** (3–31% yield). As main side reaction, we found chlorination of the arene moiety of the azobenzene, as shown by XRD in a related work (CCDC 1873980). In the last step, the compounds were treated with $POCl_3$ in the presence of 1,8-bis(dimethylamino)naphthalene (proton sponge) as base to functionalize the alcohol group. On aqueous workup, hydrolysis of the phosphorus chloride resulted in the corresponding phosphate derivatives **4a–f**.

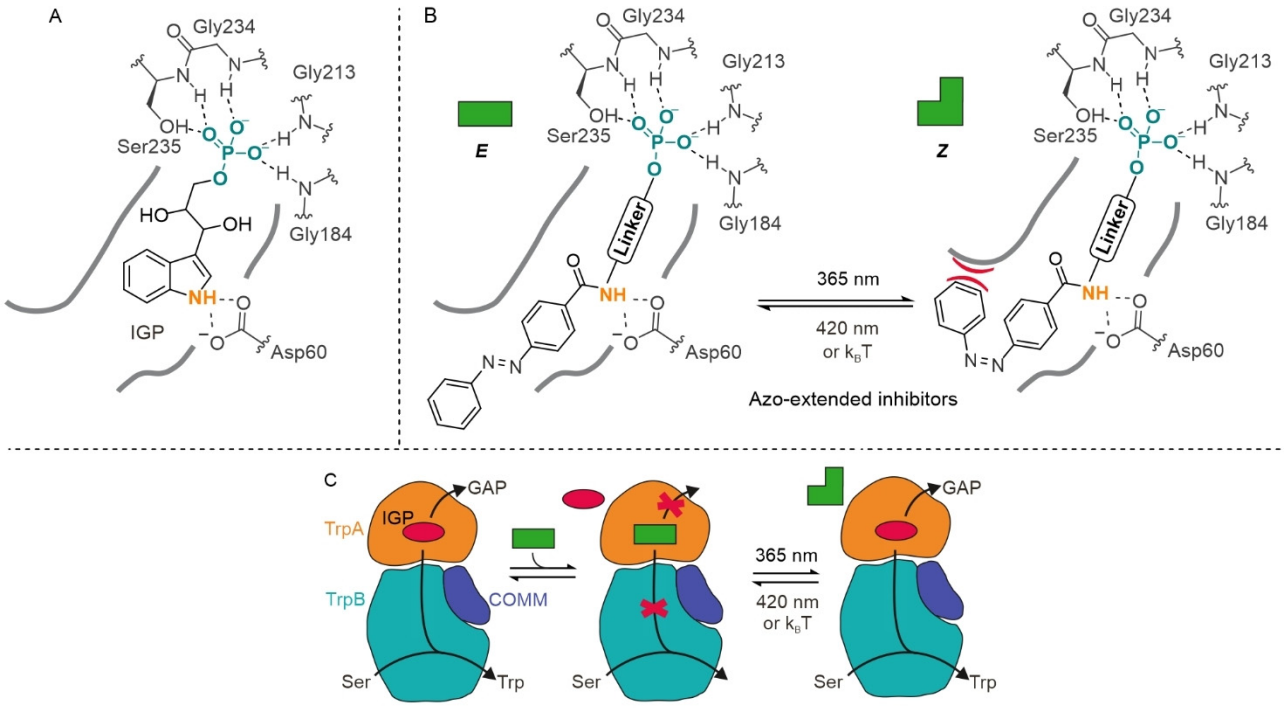

Figure 2. Design of azobenzene inhibitors of TS by the azo-extension approach. A) Binding of IGP to the active site of TrpA is mainly facilitated by two moieties. The phosphate group (cyan) interacts with the NH groups of the peptide backbone of Gly184, Gly213, Gly234, and Ser235, as well as with the side chain of Ser235. The NH group (orange) forms hydrogen bonds to the sidechain of Asp60. Gray lines indicate the dimensions of the binding pocket. B) The two main binding motifs of IGP, the phosphate and NH groups, were integrated in the design of azo-extended TS inhibitors. The phosphate group was installed at varying distances to an amide through an aryl or alkyl linker. This biologically active module was then extended with an azo moiety that switches configurations (*E*⇔*Z*; indicated by differently shaped green boxes) on irradiation with UV (365 nm) or visible (420 nm) light. While the *E* isomers are expected to bind similar to the native substrate, steric hindrance between inhibitor and binding pocket (gray) is expected to prevent binding of the *Z* isomers. C) By displacing IGP (red ellipse) from TrpA with the light-switchable azobenzene inhibitor (green box), TrpA is competitively inhibited and TrpB is deprived of its substrate indole. On irradiation with UV light, the *Z* isomer is formed. Due to its higher steric demand, we expect the *Z* isomer to show a lower binding affinity, and thus TrpA and TrpB activity is restored. This step is reversed by irradiation with visible light.

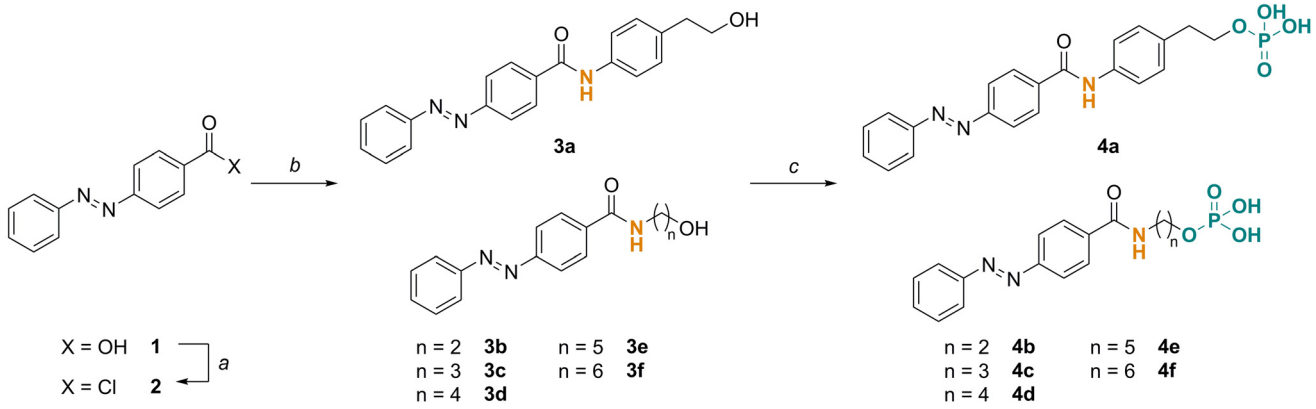

Scheme 1. Synthetic approach to photochromic TS ligands. *a*: $SOCl_2$, 80 °C, 2 h (not isolated). *b*: 4-(2-Hydroxyethyl)aniline or suitable amino alcohol (1 equiv), dry pyridine/dry $CHCl_3$ (1:5), RT, 16 h, 3–31 %. *c*: method I: 1) proton sponge (3 equiv), $POCl_3$, dry THF/dry $CHCl_3$, 0 °C to RT, 2 h; 2) acetone/water (1:1), 0.2–7 % (**4a**,**b**,**d**,**f**); method II: 1) proton sponge (3 equiv), $POCl_3$, $PO(OMe)_3$, 0 °C to RT, 2 h; 2) acetone/water (1:1), 0.5–37 % (**4c**,**e**).

After preparative HPLC purification, the compounds were isolated as orange solids. Unconverted starting material and losses during HPLC purification resulted in only low (0.2 %) to moderate (37 %) yields. Nevertheless, we obtained enough material for photophysical and photochemical studies as well as for screening of the compounds in a biochemical assay.

Photophysical and photochemical characterization

We next assessed the solubility and switching properties of our inhibitors in aqueous solution to ensure compatibility with the buffer system of our target enzyme TS. Compounds **4a**,**b**,**d**–**f** proved to be soluble, and were hence further characterized with UV/Vis spectroscopy in water (Figures S5.1–5.6 in the Supporting Information); the spectra of **4e** are shown representatively in Figure 3. Spectra were recorded at thermal equilibrium (black line), after irradiation with UV light of 365 nm (orange line), and after additional irradiation with visible light of 420 nm (green line).

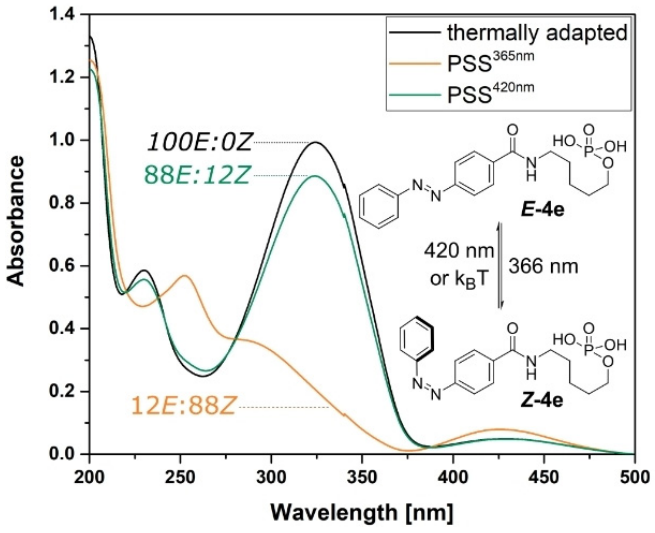

Figure 3. UV/Vis spectra of compound **4e** (65 μM) in water. The black line depicts the absorbance spectrum of the azobenzene-based inhibitor at its thermal equilibrium. The orange line represents the PSS after irradiation with light of 365 nm, and the green line shows the photostationary state after irradiation with light of 420 nm. The photostationary distribution is shown next to each line.

At thermal equilibrium, each compound exhibited a main absorbance maximum between 324 and 331 nm (Table 1), which was assigned to the ππ* transition of the *E* isomer.[23] On irradiation with 365 nm light, the photostationary state PSS^{365nm} formed; the signal of the *E* isomer decreased and simultaneously an absorbance maximum between 423 and 428 nm emerged, which was attributed to the nπ* transition of the *Z* isomer. The photostationary state distributions (PSD^{365nm}) were calculated by peak deconvolution with Gaussian functions and showed that all compounds accumulated 64–88 % of the *Z* isomer. Moreover, the metastable *Z* isomer was found to be sufficiently stable for our measurements (vide infra), as we determined a thermal lifetime of 3.76 d for compound **4e** (Figure S5.7 in the Supporting Information). Subsequent irradiation with visible light of 420 nm wavelength induced photochemical *Z*→*E* isomerization to PSS^{420nm}. However, the composition of the thermal equilibrium could not be fully regenerated—all compounds only accumulated 71–92 % of the *E* isomer (PSD^{420nm})—probably due to overlap of the nπ* band of the *E* and the nπ* band of the *Z* isomer.[23]

Table 1. Overview of photophysical and photochemical properties of compounds **4a**,**b**,**d**–**f** in water.[a]

Compound	λ_{max} (ππ* of *E*) [nm]	λ_{max} (nπ* of *Z*) [nm]	PSD^{365nm}	PSD^{420nm}
4a	331	423	36*E*:64*Z*	92*E*:8*Z*
4b	324	427	20*E*:80*Z*	71*E*:29*Z*
4d	326	428	21*E*:79*Z*	90*E*:10*Z*
4e	324	427	12*E*:88*Z*	88*E*:12*Z*
4f	325	427	15*E*:85*Z*	84*E*:16*Z*

[a] PSDs were determined by extraction of the PSS by UV/Vis spectroscopy through peak deconvolution with Gaussian functions;[27] for details, see Figures S5.1–5.6 of the Supporting Information.

Evaluation of the inhibition mode

To analyze the inhibitory potential of our compounds, we first determined the concentration range in which the azobenzenes inhibited the overall TS reaction (IGP + Ser → Trp + GAP). We

measured TS activity by monitoring tryptophan production in a recently established coupled enzymatic assay[24c] in the presence of compounds **4a**,**b**,**d–f** in their *E* or Z (referring to PSS^{365nm}) configuration. Inhibitor concentrations were gradually increased, whereas the IGP and serine concentrations were kept constant at 30 μM (≈K_M[24c]) and 5 mM (saturated[24c]), respectively. Compounds **4d–f** showed 30–70% inhibition in the low millimolar range (0.1–0.25 mM, Figure S6.1 in the Supporting Information). Compounds **4a** and **4b**, on the other hand, were not able to inhibit TS at soluble concentrations and were therefore excluded from further analyses.

We then quantified the inhibitory effect of compounds **4d–f** in their *E* and *Z* configurations. Since we designed our inhibitors as IGP analogues, we expected a competitive mode of inhibition towards the TrpA substrate (Figure 2C). Hence, we monitored IGP saturation curves for the overall TS reaction in the presence of different inhibitor concentrations. Inhibitor concentrations were chosen from the previous measurements and corresponded to 0% (0 mM), ≈30% (0.1 mM), ≈50% (0.175 mM), and ≈70% (0.25 mM) inhibition. For each IGP saturation curve, an apparent Michaelis constant K_M^{app} and an apparent rate constant k_{cat}^{app} were determined (Figure S6.2, Table S6.1 in the Supporting Information). Competitive inhibition is characterized by a decreased K_M^{app} value and an unchanged k_{cat}^{app} value; however, we observed unchanged K_M^{app} values and decreased k_{cat}^{app} values for all our compounds, and this indicates that the inhibitors did not compete with IGP for the TrpA active site.

To identify the actual mode of inhibition, we performed global fits using Equation (2) (vide infra) of the four IGP saturation curves for each inhibitor. Thus, we obtained the factor for inhibitor modality α, which indicates the mode of inhibition, and the inhibition constant K_i, which describes the strength of inhibition, for the inhibitors **4d–f** in their *E* and *Z* configurations. All compounds exhibited finite α factors indicative of a noncompetitive mode of inhibition[28] (Figure S6.2 in the Supporting Information, Table 2), which confirmed our conclusion that the azobenzene inhibitors did not compete with IGP for the TrpA active site. Although the compounds did not exhibit the intended inhibition mode, they nonetheless had K_i values in the low millimolar range (Table 2). In particular, compound **4e** stood out with K_i values of only ≈0.18 mM for its *E* isomer and ≈0.93 mM for its *Z* isomer, which correspond to a light regulation factor (LRF) of approximately five. In comparison to **4e**, the inhibitory strength of **4d** was four times weaker, represented by a higher K_i value, and the LRF of **4f** was 2.5 times lower. Compound **4e** was consequently chosen as the best candidate for the reversible light-sensitive inhibition of TS, as it combines good inhibitory strength with a high potential for light regulation.

Table 2. Inhibition values (α, K_i) and light-regulation factors for the IGP- and serine-dependent reaction of TS with compounds **4d–f** in their *E* and *Z* configurations.

Compound	Isomer	α	K_i [mM]	LRF[c]
4d	*E*[a]	4.9	0.64 ± 0.08	>6
	Z[b]	5.9×10^{-15}	>4.0	
4e	*E*[a]	0.9	0.18 ± 0.04	5
	Z[b]	0.3	0.93 ± 0.42	
4f	*E*[a]	5.0	0.05 ± 0.00	2
	Z[b]	5.4	0.10 ± 0.01	

[a] *E* refers to the compound at the thermal equilibrium containing approximately 100% *E* isomer. [b] *Z* refers to the compound with the *Z*-enriched PSD after irradiation with UV light. [c] LRF = light-regulation factor. Values for K_i ± standard error were determined by fitting the substrate saturation curves for four different inhibitor concentrations (Figure S6.2 in the Supporting Information) with Equation (2) (vide infra).

We further tested whether the azobenzene inhibitors might associate with the hydrophobic binding site of indole in TrpB instead of the active site of TrpA. Hence, we measured the TrpB reaction (indole + Ser → Trp) with varying concentrations of indole and saturating concentrations of serine in the presence of our best inhibitor **4e**. The K_M^{app}, k_{cat}^{app}, K_i, and α values were determined accordingly (Figure S6.3, Table S6.2 in the Supporting Information). Similar to the inhibition studies with IGP, the K_M^{app} values remained unchanged, whereas the k_{cat}^{app} values decreased with increasing inhibitor concentrations. Consistently, the α factors for both isomers were finite (≈0.7), indicating that compound **4e** does not compete with indole for binding at the TrpB active site. Furthermore, **4e** showed K_i values of approximately 0.18 mM for its *E* isomer and approximately 0.50 mM for its *Z* isomer, corresponding to an LRF of approximately three, comparable to the measurements with IGP. These results demonstrate that the inhibitory mode of our light-switchable azobenzene inhibitors is also noncompetitive towards the TrpB active site.

In conclusion, other than originally intended, our synthesized azobenzene-based compounds led to noncompetitive inhibition of TS activity. Nevertheless, inhibition strength could still be light-regulated for all our inhibitors by a factor of 2–6. The *E* configuration conferred a stronger inhibitory effect suggesting that this isomer associates more easily with the TS complex than the sterically more demanding *Z* isomer. Moreover, increasing length of the alkyl linker in **4d–f** resulted in increasingly stronger inhibition; however, it also reduced the potential for light-responsive inhibition. Our best inhibitor **4e** showed both a relatively large inhibition constant for the *E* isomer of 0.18 mM and a relatively high LRF. Previously reported TS inhibitors that bind at the TrpA active site or close to the protein interface showed high or even ultrahigh inhibition strengths with K_i values of 4.8 μM[29] and 40 nM,[16] respectively. In comparison, **4e** only shows medium-strength inhibition, which is expected to have at best a slightly harmful effect on bacteria. However, taking into account that this inhibitor was not designed for a noncompetitive inhibition mode, inhibition in the low millimolar range is still noteworthy. We reasoned that, by identifying the exact binding site of **4e**, we might be able to optimize the structure of this lead compound, and hence its inhibition strength, in future studies.

Cocrystallization of TS with azobenzene inhibitor 4e

For identification of the binding site of **4e** in the TS complex, we performed cocrystallization experiments. To ensure that TS

was uniformly loaded with **4e** in the crystallization setup, we first determined the binding constant K_D of the inhibitor to the TS complex. Isothermal titration calorimetry (ITC) provided a K_D value of approximately 67 μM indicating strong binding of **4e** to the TS complex (Figure S7.1 in the Supporting Information). Additionally, we measured the K_D values of **4e** to the isolated subunits, obtaining K_D values of approximately 130 μM for TrpA and approximately 10 μM for TrpB (Figures S7.2 and S6.3 in the Supporting Information). Thus, **4e** binds to TrpB with significantly higher affinity. We therefore expected that the binding site of **4e** was located in the TrpB subunit. Following this analysis, we crystallized the TS complex in the presence of **4e** at saturated concentration (≈750 μM) and in excess (ca. twofold) over the enzyme and solved its structure (TS_{4e}) with approximately 2.5 Å resolution (PDB-ID: 7A20; Table S7.1 in the Supporting Information). The TS_{4e} structure contained two chain pairs of the functional unit of TS per unit cell. Since crystallization took several weeks, we expected to find the *E* isomer instead of the thermally unstable *Z* isomer of **4e** (vide supra). However, no electron density could be assigned to the inhibitor. The high binding affinity of **4e** to the TS complex and the high concentrations used for the crystallization experiments led to the conclusion that **4e** was bound to the TS complex but could not be resolved, which suggested highly dynamic behavior of **4e** in the binding site.

We compared TS_{4e} with an active conformation and an inactive conformation of TS to identify potential structural changes induced by **4e** (Figure 4). In the structure of the active TS (TS_{AA}; blue)[13a] an IGP analogue is bound to TrpA, the aminoacrylate intermediate is bound to TrpB, and the COMM domain adopts a "closed" conformation. In the structure of the inactive TS (TS_{IA}; gray),[30] internal aldimine is bound to TrpB, and the COMM domain adopts an "open" conformation. In TS_{4e} (red), no significant structural differences were found in the TrpA subunit and the core structure of the TrpB subunit (Figure 4A). However, the COMM domain is even further shifted towards an "extended-open" conformation (Figure 4B). Notably, the PLP cofactor was missing in the TrpB active site, and instead a single buffer molecule was detected, that is, the TrpB active site is exposed to solvent.

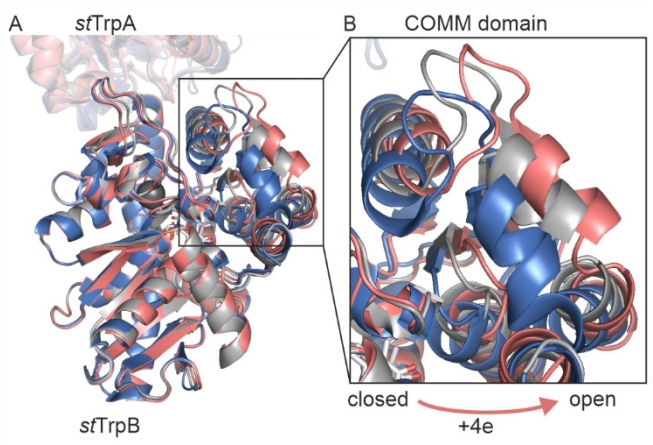

Figure 4. Structural comparison of TS in the presence of **4e** (red; PDB-ID: 7A20, chain pair AB) with the fully active aminoacrylate bound TS_{AA} (blue; PDB-ID: 2J9X, chain pair AB), and the inactive internal aldimine bound TS_{IA} (gray; PDB-ID: 1BKS, chain pair AB). A) Superposition of the three structures. No structural differences were observed in the TrpA subunit (top, transparent) and the core of the TrpB subunit (bottom). B) **4e** induced significant conformational changes in the COMM domain. While the COMM domain adopts a closed conformation in TS_{AA} (blue) and an open conformation in TS_{IA} (gray), it is extended-open in the presence of **4e** (red).

These findings suggest that **4e** holds the TS complex in an unproductive conformation defined by an extended-open COMM domain. Similar observations were made by Arnold and co-workers in their studies on TS from *Pyrococcus furiosus*. They found that a single molecule of β-methyl tryptophan bound to a solvent-accessible binding cleft close to the TrpB active site led to an extended-open state,[31] that is, the COMM domain was shifted away from the protein core, similar to our extended-open conformation induced by **4e**. This conformation of the COMM domain in TS_{4e} most likely prohibits the allosteric communication between the two active sites and renders both enzymes inactive. In addition, access to the TrpB active site is opened by the inhibitor, so that it is unprotected against entry of solvent. These effects of **4e** on the TS structure explain the noncompetitive mode of inhibition. However, it is still unclear where the binding site of the inhibitor is located and how the inhibitor causes these changes. Since **4e** showed the highest affinity toward the TrpB subunit in binding studies, and since it strongly affected the COMM domain and the TrpB active site in crystallization studies, we continued to search for the binding site in the TrpB subunit by a computational approach.

Computational analysis of the putative inhibitor binding site

Even though electron density cannot be detected when a ligand is too dynamic, the binding site can still be traced by identifying pockets in the protein structure that are large enough to accommodate the ligand. Therefore, we analyzed the structures of TS_{AA}, TS_{IA}, and TS_{4e} with the software tool Mole2.5.[32] In TS_{AA}, in which the COMM domain exhibits a closed conformation, no significantly large pockets could be found (Figure S8.1.A in the Supporting Information). However, in TS_{IA}, in which the COMM domain takes on an open conformation, we identified a surface-accessible cavity with a length of approximately 25 Å, located in the cleft between the COMM domain and the TrpB active site (Figure S8.1.B–C in the Supporting Information). Finally, in TS_{4e}, in which the COMM domain is extended-open, we also found a cavity at the same location as in TS_{IA} but slightly enlarged with a length of approximately 29 Å (Figure 5A). This cavity matches the dimensions of the inhibitor (length ≈21 Å) and exists in both TrpB chains of TS_{4e} with highly similar size and shape. Binding of our inhibitor to this potential binding site could explain the highly impaired structure of TS_{4e} with the COMM domain in an extended-open conformation. Remarkably, β-methyl tryptophan was also bound very close to this binding site when inducing the extended-open state of TS in previous studies, and this suggests that this site might be a novel allosteric binding site of TS.[31] In agreement with this, binding of **4e** led to a

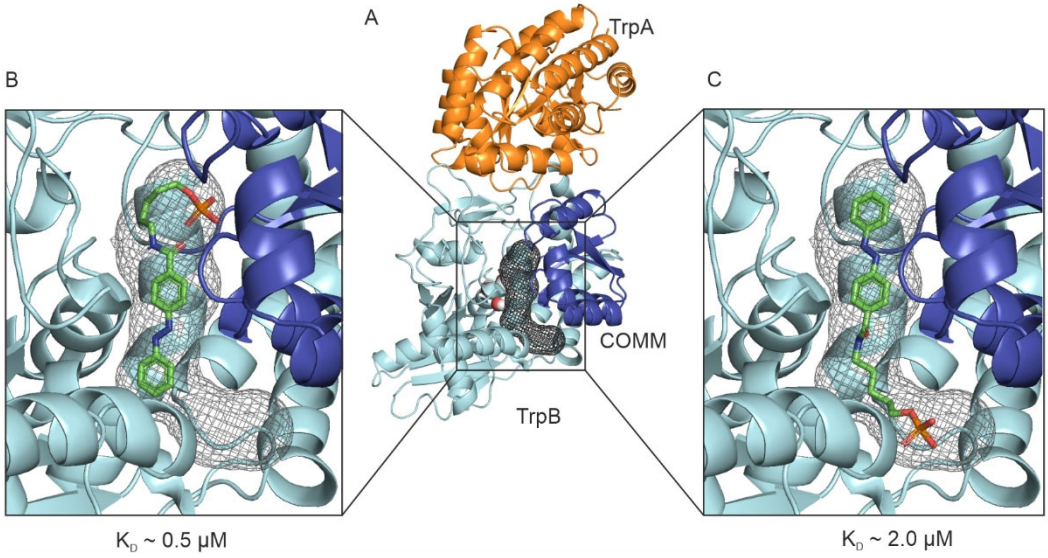

Figure 5. Identification of the **4e** binding site in TS. A) Mole2.5[32] analysis of TS_{4e} (PDB-ID: 7A20) identified a pocket (gray mesh) between the TrpB active site (marked with the bound buffer molecule in spheres) and the COMM domain (blue) that matches the dimensions of the inhibitor. Note: the cavity is only shown for the chain pair CD; however, it also forms in the chain pair AB. B), C) Docking analysis with YASARA[33] demonstrated that **4e** (green) can bind in various orientations in the binding pocket identified in A) (black); two variations, which represent the binding orientations of cluster 1 (B) and cluster 3 (C), are shown with their predicted K_D values.

noncompetitive mode of inhibition with respect to both the TrpA and TrpB active sites. To the best of our knowledge, this binding site has so far been unexplored in inhibition studies. Two other groups described similarly allosteric inhibitors, but their binding site is located within the indole channel and closer to the TrpA:TrpB interface.[15,16]

Continuing our computational examination, we tested whether **4e** could sterically fit into this cavity and interact with the lining residues. To this end, we performed a docking analysis using YASARA.[33] In this experiment, the protein conformation was kept fixed, while the inhibitor was docked with full conformational freedom. As a result, 17 binding geometries could be identified for the inhibitor, out of which ten had predicted K_D values below 5 μM (Table S8.1, Figure S8.2, Figure S8.3 in the Supporting Information). Remarkably, the orientation of **4e** in most of the binding geometries differed significantly, as illustrated by two exemplary orientations in Figure 5B and C, which exhibited predicted K_D values of 0.5 and 2.0 μM. In these examples, the phosphate group is buried at the deep end of the cavity (Figure 5B) or points towards the surface of the protein (Figure 5C). This variety of putative inhibitor geometries in the binding pocket confirms a highly dynamic binding behavior of **4e**, and is therefore consistent with the lack of electron density in the crystal structure.

Photocontrolling the noncompetitive inhibition of TS

Our findings showed that inhibitor **4e**, which was originally designed to associate at the TrpA active site, most likely binds to a cavity between the TrpB active site and the COMM domain, and shifts the latter into an unproductive extended-open conformation. In this way, **4e** might also block the hydrophobic channel, which is located close to its binding site, and thus impede indole transport from the TrpA active site to the TrpB active site. As a result, the light-sensitive inhibition of TS by **4e** is noncompetitive. Hence, a revision of our proposed strategy of light-dependent inhibition of TS (Figure 2C) was required.

In the absence of the inhibitor, the allosteric communication between the TrpA and TrpB active sites can take place, activating the turnover of IGP in TrpA and serine in TrpB (Figure 6A, left panel). The *E* isomer of **4e** binds with high affinity to the TrpB subunit and disturbs the allosteric communication by shifting the COMM domain to the extended-open conformation, rendering TrpB, and most likely TrpA, inactive (Figure 6A, middle panel). As confirmed by inhibition studies, the *Z* isomer, obtained by irradiation with UV light, has lower apparent binding affinity and dissociates from the TrpB subunit. Thus, the active, closed conformation of the COMM domain is reconstituted, the allosteric communication is restored, and TrpA and TrpB are both reactivated (Figure 6A, right panel).

We further evaluated this sequence of events in an in situ irradiation setup (Figure 6B) by monitoring the activity of the overall TS reaction in three samples. One reaction assay was performed in the presence of inhibitor **4e** in its *E* configuration in the dark ("dark"). The second assay was started in the presence of inhibitor **4e** in its *E* configuration, and then irradiated during the initial linear activity phase of the enzyme ("direct photocontrol"). Moreover, we applied the same treatment as control to a reaction assay in the absence of **4e** ("uninhibited"). TS activity was inhibited approximately twofold by **4e** in the dark and direct-photocontrol (prior to irradiation) samples relative to the activity in the uninhibited sample. This confirmed the medium-strength inhibition effect observed in inhibitory studies and depicted in the middle panel of Figure 6A. On irradiation of the direct-photocontrol sample, the reaction velocity increased 1.2-fold. This LRF is unexpectedly small and disagrees with the LRF determined in K_i studies. However, TS

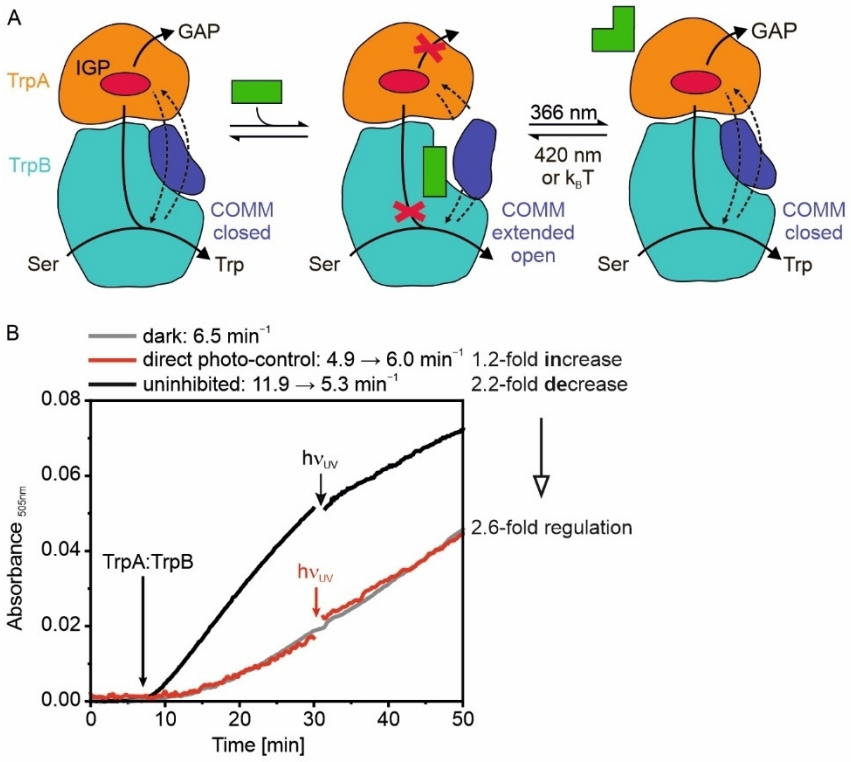

Figure 6. Activity modulation of TS by the photoswitchable noncompetitive inhibitor **4e**. A) Binding of **4e** in its *E* configuration (green rectangle) to TrpB shifts the COMM domain to an extended-open conformation, which likely disrupts the allosteric activation between TrpA and TrpB and thus diminishes tryptophan production from IGP (red ellipse) and Ser. On irradiation with UV light, the inhibitor is isomerized to its *Z* configuration (green elbow), which restores TrpA and TrpB activity. This step is reversed by irradiation with visible light. B) Direct photocontrol of TS activity with **4e** (red) compared to a dark control (kept in the dark; gray) and an uninhibited control (in the absence of **4e**, black). Reaction conditions: 50 mM potassium phosphate pH 7.5, 100 mM KCl, 5 mM L-serine, 3.0 mM phenol, 3.0 mM 4-aminoantipyrine, 20 μM PLP, 0.075 g L^{-1} HRP, 1.0 g L^{-1} VioA, and, in the case of direct photocontrol and dark, 250 μM **4e**. All three reactions were started with the TS complex (0.1 μM), monitored for approximately 30 min, irradiated for 15 s at 365 nm while enzyme velocity was still in the initial linear range, and monitored further up to 50 min.

activity in the absence of **4e** in our uninhibited sample was decreased by a factor of 2.2 on irradiation with UV light. We previously observed this effect during our studies on light control of TS with photosensitive unnatural amino acids,[24c] and associated it with degradation of the light-sensitive PLP cofactor. When we now consider this additional phototoxic effect, light-induced isomerization of **4e** actually translates into a 2.6-fold regulation of TS activity, approximating the LRF of about 5 in the K_i studies. This recovery of enzyme activity constitutes the situation depicted in the right panel of Figure 6A.

An LRF of 3–5 sets high expectations for the inhibitor's effect on bacterial growth. In general, photochromic inhibitors of enzymes are often more convincing in vivo than in vitro.[17b] This holds true particularly for enzymes in signaling cascades, but also for antibacterial lead compounds, for which it could be shown that an LRF of approximately two is sufficient to control bacterial death with light.[34] The photocontrolled effect of **4e** on the essential multi-enzyme complex TS of *S. typhimurium* is therefore promising, but various improvements are necessary before its efficacy against bacteria can be proved and ultimately its antibiotic potential can be tested in vivo. First, binding and inhibition strengths need to be increased to improve the effectiveness of the inhibitor in biological systems. For this, the structure of the azobenzene-based compound can be customized for binding to the cavity between the TrpB active site and the COMM domain. Motifs for the specific interaction with residues lining the cavity can be introduced into the linker region or might replace it. Moreover, the irradiation wavelength needs to be shifted towards higher regions of the electromagnetic spectrum, for example, in the red region of visible light, to increase the penetration depth of light and minimize phototoxic effects on the tissue. The hazardous effect of UV light was emphasized by the strong decrease of TS activity after irradiation. The irradiation wavelength, PSD, and thermal lifetime of the *Z* isomer can be optimized by introducing suitable substituents[35] or by applying heteroaryl design.[36] Ultimately, the photocontrollable inhibitor can be deployed to tackle common drawbacks of customary antibiotics. These are especially the collateral damage that they cause, for example, by attacking pathogenic and nonpathogenic bacteria, and their permanent biological activity. As a consequence, accumulation of these drugs in the environment promotes the creation and rapid spreading of multiresistance in bacterial strains.[37] Hence, a spatiotemporally restricted mode of the antibacterial efficacy of antibiotics is desirable. Our inhibitor **4e** is not yet suited for this purpose, as the less inhibitory *Z* isomer is also the thermally unstable one. Consequently, the amount of the more-inhibitory *E* isomer would be increased over time. However, by, for example, applying the sign-inversion strategy the thermodynamic stability of the two

photoisomers could be inverted to make the strongly inhibitory *E* isomer the metastable form.[38]

Conclusion

Despite an urgent need, the search for new antibiotics was only recently expanded to inhibitors that target metabolic enzymes or that can be controlled externally. Following this research direction, we set out to explore the TS of *S. typhimurium* as a potential antibiotic target enzyme by designing an inhibitor that can be controlled in a spatiotemporal manner by light. Hence, we synthesized a small library of azobenzene-based inhibitors towards the TrpA subunit. The compounds can be reversibly switched in water up to approximately 90% of the photochemically generated isomer by using UV or blue light. Inhibition studies quickly identified **4e** as the most promising TS inhibitor, as it provides exceptionally good solubility, distinct photochromism, reasonable inhibition, and a pronounced difference in inhibition strength between the photoisomers. This analysis also revealed a noncompetitive mode of inhibition towards both the TrpA and TrpB active sites, a finding contrary to our design. We consequently used a combination of ITC-based binding studies, crystallization experiments, and computational analyses to unveil the potential binding site of **4e**, which is a cavity at the TrpB subunit. Moreover, structural analysis showed pronounced conformational changes of the COMM domain, which adopted an allosterically unproductive extended-open conformation. In further studies, we aim to improve the design of this new lead compound, taking the characteristics of its actual binding site into account, and to optimize the photophysical and photochemical properties of the parent azobenzene. These findings are the starting point to develop fully light-controllable TS inhibitors, which can be further optimized into smart antibiotic agents.

Experimental Section

General information

Analytical samples of the alcohols and final compounds were purified by preparative HPLC [MeCN in H_2O/0.05% trifluoroacetic acid (TFA) 5–100% over 20 min] to give all compounds as orange solids. NMR spectra were recorded with a Bruker Avance 400 MHz NMR or a Bruker Avance 600 Kryo. Some of the alcohols partly decomposed during the measurement. Thus, carbon signals were assigned by means of HSQC measurements (quaternary carbon atoms could not be assigned in these cases). Due to the low reaction yields, ^{13}C NMR spectroscopy was not feasible for **4a**–**d**,**f**. A description of the general working methods can be found in Section 1 of the Supporting Information.

Synthesis

General procedure for amide formation: In a crimp-top vial, (*E*)-4-(phenyldiazenyl)benzoic acid (1 equiv) was dissolved in $SOCl_2$ (1 mL per 200 mg). The suspension was heated to 80 °C for 2 h to give a clear, red solution. The reaction mixture was cooled to ambient temperature and the solvent was removed in vacuo. The vial was flushed with vacuum/nitrogen three times and dry $CHCl_3$ (5 mL) was added under nitrogen atmosphere. Then, a solution of the respective aniline (1 equiv) or amino alcohol (1 equiv), in dry pyridine (1 mL) was added dropwise through a syringe. The solution was stirred for 16 h and the solvent was removed in vacuo. The crude product was purified by MPLC (20→100% EtOAc in petroleum ether).

(E)-N-(4-(2-hydroxyethyl)phenyl)-4-(phenyldiazenyl)benzamide (***3a***): (*E*)-4-(Phenyldiazenyl) benzoic acid (4.42 mmol) was employed. Compound **3a** was obtained in 8% yield (0.37 mmol). R_f (10% MeOH in CH_2Cl_2): 0.6. ^{1}H NMR (300 MHz, 10% CD_3OD in $CDCl_3$): δ = 8.03 (d, J = 8.5 Hz, 2H), 7.98–7.93 (m, 2H), 7.92–7.89 (m, 2H), 7.57 (d, J = 8.3 Hz, 2H), 7.53–7.45 (m, 3H), 7.19 (d, J = 8.4 Hz, 2H), 3.76 (t, J = 6.9 Hz, 2H), 2.80 (t, J = 6.9 Hz, 2H). ^{13}C NMR (151 MHz, [D_6]acetone): δ = 132.0 (+), 130.3 (+), 130.1 (+), 129.6 (+), 123.8 (+), 123.4 (+), 121.1 (+), 64.0 (−), 30.4 (−). Assignment was based on HSQC measurements due to low concentrations and lability of the compound. Thus, quaternary carbon atoms could not be assigned. IR: $\tilde{\nu}$ = 3351(m), 3045 (w), 2926 (w), 2863 (w), 1648 (s), 1520 (s), 1051 (m), 861 (m), 820 (m), 771 (m), 686 cm^{-1} (m). ESI-MS: calcd: 345.1477, found: 713.3 (2*M*Na$^+$, 5%; 368.1 *M*Na$^+$, 10%; 346.2 *M*H$^+$, 100%). HRMS (ESI): found: 368.1373 (*M*Na$^+$, 15%), 346.1559 (*M*H$^+$, 100%).

(E)-N-(2-hydroxyethyl)-4-(phenyldiazenyl)benzamide (***3b***): (*E*)-4-(Phenyldiazenyl)benzoic acid (4.42 mmol) was employed. Compound **3b** was obtained in 31% yield (1.39 mmol). R_f (10% MeOH in CH_2Cl_2): 0.5. ^{1}H NMR (400 MHz, [D_6]acetone): δ = 8.10–8.05 (m, 2H), 7.98–7.90 (m, 4H), 7.60–7.51 (m, 3H), 3.68 (t, J = 5.7 Hz, 2H), 3.50 (q, J = 5.6 Hz, 2H). ^{13}C NMR (151 MHz, [D_6]acetone): δ = 129.5 (+), 129.2 (+), 128.2 (+), 122.7 (+), 122.3 (+), 60.8 (−), 42.5 (−). Assignment was based on HSQC measurements due to low concentrations and decomposition of the compound during the extended measuring time. Thus, quaternary carbon atoms could not be assigned. IR: $\tilde{\nu}$ = 3258 (w), 3064 (w), 3926 (w), 1722 (m), 1626 (m), 1268 (s), 1092 (m), 857 (m), 686 cm^{-1} (s). ESI-MS: calculated: 269.1164, found: 561.2 (2*M*Na$^+$, 20%), 292.1 (*M*Na$^+$, 20%), 270.1 (*M*H$^+$, 100%). HRMS (ESI): found: 292.1062 (*M*Na$^+$, 20%), 270.1242 (*M*H$^+$, 100%).

(E)-N-(3-hydroxypropyl)-4-(phenyldiazenyl)benzamide (***3c***): (*E*)-4-(Phenyldiazenyl)benzoic acid (2.10 mmol) was employed. Compound **3c** was obtained in 10% yield (0.22 mmol). R_f (10% MeOH in CH_2Cl_2): 0.5. ^{1}H NMR (400 MHz, [D_6]acetone): δ = 8.16–8.06 (m, 2H), 8.03–7.87 (m, 4H), 7.75–7.47 (m, 3H), 3.64 (t, J = 6.0 Hz, 2H), 3.55 (q, J = 6.5 Hz, 2H), 1.80 (p, J = 6.3 Hz, 2H). ^{13}C NMR (101 MHz, [D_6]acetone): δ = 166.1 (q), 153.9 (q), 152.5 (q), 137.1 (q), 131.7 (+), 129.3 (+), 128.3 (+), 122.8 (+), 122.5 (+), 59.1 (−), 36.9 (−), 32.5 (−). IR: $\tilde{\nu}$ = 3368 (w), 3291 (m), 3060 (w), 2937 (w), 2881 (w), 1627 (s), 1536 (s), 1073 (m), 775 (m), 686 (s). ESI-MS: calculated: 283.1324, found: 306.1 (*M*Na$^+$, 20%), 284.1 (*M*H$^+$, 100%). HRMS (ESI): found: 306.1215 (*M*Na$^+$, 20%), 284.1401 (*M*H$^+$, 100%).

(E)-N-(4-hydroxybutyl)-4-(phenyldiazenyl)benzamide (***3d***): (*E*)-4-(Phenyldiazenyl)benzoic acid (2.21 mmol) was employed. Compound **3d** was obtained in 3% yield (0.06 mmol). R_f (10% MeOH in CH_2Cl_2): 0.5.^{1}H NMR (400 MHz, [D_6]acetone): δ = 8.11–8.06 (m, 2H), 7.99–7.93 (m, 4H), 7.63–7.55 (m, 3H), 3.59 (t, J = 6.2 Hz, 2H), 3.51–3.39 (m, 2H), 1.78–1.66 (m, 2H), 1.66–1.55 (m, 2H). ^{13}C NMR (101 MHz, [D_6]acetone): δ = 165.5 (q), 153.8 (q), 152.5 (q), 137.4 (q), 131.7 (+), 130.8 (+), 129.3 (+), 128.2 (+), 122.8 (+), 122.4 (+), 61.3 (−), 39.6 (−), 30.2 (−), 26.2 (−). IR: $\tilde{\nu}$ = 3321 (w), 3045 (w), 2926 (w), 2862 (w), 1647 (s), 1521 (s), 861 (m), 820 (s), 771 (s), 865 cm^{-1} (s). ESI-MS: calculated: 297.1477, found: 617.3 (2*M*Na$^+$, 40%), 320.1 (*M*Na$^+$, 20%), 298.2 (*M*H$^+$, 100%). HRMS: 320.1376 (*M*Na$^+$, 40%), 298.1559 (*M*H$^+$, 100%).

*(E)-N-(5-hydroxypentyl)-4-(phenyldiazenyl)benzamide (**3e**)*: (*E*)-4-(Phenyldiazenyl)benzoic acid (1.33 mmol) was employed. Compound **3e** was obtained in 5% yield (0.07 mmol). R_f (10% MeOH in CH_2Cl_2): 0.8. ^{1}H NMR (400 MHz, [D$_6$]acetone): δ = 8.11–8.05 (m, 2H), 7.99–7.94 (m, 4H), 7.63–7.56 (m, 3H), 3.54 (t, J = 6.3 Hz, 2H), 3.47–3.40 (m, 2H), 1.65 (p, J = 7.2 Hz, 2H), 1.59–1.51 (m, 2H), 1.51–1.42 (m, 2H). ^{13}C NMR (151 MHz, [D$_6$]acetone): δ = 130.2 (+), 129.3 (+), 128.2 (+), 122.8 (+), 122.4 (+), 62.3 (−), 40.5 (−), 33.4 (−), 29.4 (−), 24.1 (−). Assignment was based on HSQC measurements due to low concentrations and decomposition of the compound during the extended measuring time. Thus, quaternary carbon atoms could not be assigned. IR: $\tilde{\nu}$ = 3295 (w), 3052 (w), 2933 (w), 2870 (w), 1714 (s), 1629 (s), 1536 (s), 1271 (s), 1119 (m), 775 (s), 686 (s). ESI-MS: calculated: 311.1634, found: 312.2 (*M*H$^+$, 100%). HRMS: 334.1531 (*M*Na$^+$, 40%), 312.1712 (*M*H$^+$, 100%).

(E)-N-(6-hydroxyhexyl)-4-(phenyldiazenyl)benzamide (**3f**): (*E*)-4-(Phenyldiazenyl) benzoic acid (4.32 mmol) was employed. **3a** was obtained in 2% yield (0.07 mmol). R_f (10% MeOH in CH_2Cl_2): 0.5. ^{1}H NMR (400 MHz, [D$_6$]acetone): δ = 8.10–8.06 (m, 2H), 8.00–7.93 (m, 4H), 7.65–7.53 (m, 3H), 3.53 (t, J = 6.4 Hz, 2H), 3.43 (td, J = 7.2, 5.8 Hz, 2H), 1.64 (p, J = 7.1 Hz, 2H), 1.56–1.48 (m, 2H), 1.45–1.36 (m, 4H). ^{13}C NMR (151 MHz, [D$_6$]acetone): δ 152.8 (+), 152.5 (+), 131.7 (+), 129.3 (+), 128.3 (+), 122.8 (+), 122.4 (+), 62.4 (−), 40.6 (−), 33.8 (−), 30.7 (−), 30.6 (−), 27.2 (−). Assignment was based on HSQC measurements due to low concentrations and decomposition of the compound during the extended measuring time. Thus, quaternary carbon atoms could not be assigned. IR: $\tilde{\nu}$ = 3384 (w), 3295 (m), 2937 (m), 2855 (m), 1627 (s), 1531 (s), 1297 (m), 858 (m), 775 (s), 686 cm^{-1} (s). ESI-MS: calculated: 325.1790, found: 673.3 (2*M*Na$^+$, 25%), 348.2 (*M*Na$^+$, 35%), 326.2 (*M*H$^+$, 100%). HRMS: 348.1687 (*M*Na$^+$, 20%), 326.1869 (*M*H$^+$, 100%).

Phosphorylation

General procedure I for phosphorylation: An oven-dried crimp-top vial was loaded with compound **3a**,**b**,**d**,**f** (1 equiv), proton sponge (3 equiv), and a stirring bar, and sealed. The vial was purged with vacuum/nitrogen (3× each) before dry $CHCl_3$ (1 mL per 0.15 mmol) was added. The reaction mixture was cooled to 0 °C and $POCl_3$ in dry THF (1:2, 0.5 mL per 0.15 mmol) was added dropwise via syringe. Then, the mixture was allowed to warm to ambient temperature and was stirred for 2 h. After quenching with acetone/water (1:1), the solvent was removed in vacuo and the crude product was purified through preparative HPLC (MeCN in H_2O/0.05% TFA, 5→95%). The products were obtained as orange powders after lyophilization.

General procedure II for phosphorylation: An oven-dried crimp-top vial was equipped with compound **3c**,**e** (1 equiv), proton sponge (3 equiv), and a stirring bar, and sealed. The vial was purged with vacuum/nitrogen (3× each) before $PO(OMe)_3$ (1 mL per 0.15 mmol) was added. The reaction mixture was cooled to 0 °C and $POCl_3$ (0.5 mL per 0.15 mmol) was added dropwise by syringe. Then, the mixture was allowed to warm to ambient temperature and was stirred for 2 h. After quenching with acetone/water (1:1), the solvent was removed in vacuo and the crude product was purified by preparative HPLC (MeCN in H_2O/0.05% TFA, 5→95%). The products were obtained as orange powders after lyophilization.

*(E)-4-(4-(phenyldiazenyl)benzamido)phenethyl dihydrogenphosphate (**4a**)*: Compound **3a** (125 mg, 0.36 mmol) was employed. Compound **4a** was obtained in 0.5% yield (0.8 mg, 0.002 mmol). HPLC: R_t = 15.7 min, >99% purity (220 nm), 96% purity (254 nm trace). ^{1}H NMR (400 MHz, CD_3ODCD_3OD): δ = 8.11 (d, J = 8.5 Hz, 2H), 8.02 (d, J = 8.5 Hz, 2H), 7.96 (dd, J = 7.9, 1.9 Hz, 2H), 7.65 (d, J = 8.3 Hz, 2H), 7.60–7.54 (m, 3H), 7.30 (d, J = 8.4 Hz, 2H), 4.14 (q, J = 7.0 Hz, 2H), 2.98 (t, J = 7.0 Hz, 2H). ^{31}P NMR (162 MHz, CD_3OD): δ = 0.00. IR: $\tilde{\nu}$ = 2922 (w), 2662 (w), 1647 (m), 1524 (m), 1062 (s), 771 (s), 686 (s). ESI-MS: calculated: 425.1141, found: 426.1 (*M*H$^+$, 55%), 380.1 (50%), 346.2 (100%), 309.1 (50%), 224.1 (30%); found: 424.1 ((*M*−H)$^-$, 100%), 344.1 (30%). HRMS: 426.1210 (*M*H$^+$, 100%), 424.1079 ((*M*−H)$^-$, 100%).

*(E)-2-(4-(phenyldiazenyl)benzamido)ethyl dihydrogen phosphate (**4b**)*: Compound **3b** (374 mg, 1.38 mmol) was employed. **4b** was obtained in 0.2% yield (1.2 mg, 0.003 mmol). ^{1}H NMR (400 MHz, CD_3OD): δ = 8.07–7.89 (m, 6H), 7.62–7.48 (m, 6H), 3.79–3.69 (m, 4H). ^{31}P NMR (162 MHz, CD_3OD): δ = −0.00. ESI-MS: calculated: 349.0828. found: 348.1 ((*M*−H)$^-$, 100%). IR: $\tilde{\nu}$ = 3299 (w), 2963 (w), 2930 (w), 1629 (s), 1536 (s), 861 (s), 775 (s), 686 (s).

*(E)-3-(4-(phenyldiazenyl)benzamido)propyl dihydrogen phosphate (**4c**)*: Compound **3c** (63 mg, 0.22 mmol) was employed. Compound **4c** was obtained in 7% yield (5.3 mg, 0.02 mmol). HPLC: R_t = 18.1 min, 95% purity (220 and 254 nm). ^{1}H NMR (400 MHz, CD_3OD): δ = 8.69 (s, 0H), 8.08–7.89 (m, 1H), 7.69–7.41 (m, 1H), 3.67 (t, J = 6.5 Hz, 0H), 3.56 (tt, J = 6.9, 2.9 Hz, 0H), 2.10 (p, J = 6.7 Hz, 0H). ^{31}P NMR (162 MHz, CD_3OD). δ = 0.00. IR: $\tilde{\nu}$ = 3317 (w), 3079 (w), 2937 (w), 2463 (w), 1625 (m), 1543 (m), 1442 (m), 1286 (m), 857 (m), 775 (s), 686 (s). ESI-MS: calculated: 347.3108. found: 346.1 ((*M*−H)$^-$, 100%).

*(E)-4-(4-(phenyldiazenyl)benzamido)butyl dihydrogen phosphate (**4d**)*: Compound **3d** (293 mg, 0.99 mmol) was employed. Compound **4d** was obtained in 4% yield (14.7 mg, 0.04 mmol). HPLC: R_t = 18.7 min, 97% purity (220 nm), 95% purity (254 nm). ^{1}H NMR (400 MHz, CD_3OD): δ = 8.18–8.06 (m, 4H), 8.03–7.96 (m, 2H), 7.63–7.56 (m, 3H), 4.90 (t, J = 5.4 Hz, 2H), 3.80 (t, J = 6.0 Hz, 2H), 2.46–2.32 (m, 2H). ^{31}P NMR (162 MHz, CD_3OD): δ = 0.00. IR: $\tilde{\nu}$ = 3414 (w), 3029 (w), 1662 (s), 1275 (m), 1178 (s), 1115 (s), 690 (s). ESI-MS: calculated: 377.1141, found: 378.1 (*M*H$^+$, 100%), 247.3 (80%), 223.1 (30%); found: 376.1 ((*M*−H)$^-$, 100%). HRMS: 378.1215 (*M*H$^+$, 100%), 376.1078 ((*M*−H)$^-$, 100%).

*(E)-5-(4-(phenyldiazenyl)benzamido)pentyl dihydrogen phosphate (**4e**)*: Compound **3e** (184 mg, 0.59 mmol) was employed. Compound **4e** was obtained in 37% yield (86.7 mg, 0.22 mmol). HPLC: R_t = 13.4 min, 98% purity (220 nm), <99% purity (254 nm). ^{1}H NMR (400 MHz, CD_3OD): δ = 8.04–7.73 (m, 6H), 7.51–7.12 (m, 3H), 3.89 (q, J = 6.5 Hz, 2H), 3.30 (t, J = 7.1 Hz, 2H), 1.70–1.48 (m, 4H), 1.40–1.28 (m, 2H). ^{13}C NMR (101 MHz, CD_3OD): δ = 168.0 (q), 154.1 (q), 152.5 (q), 136.4 (q), 131.5 (+), 129.0 (+), 128.0 (+), 122.6 (+), 122.4 (+), 66.2 (−), 39.6 (−), 29.8 (−), 28.6 (−), 22.7 (−).^{31}P NMR (162 MHz, CD_3OD): δ = 0.16. IR: $\tilde{\nu}$ = 3313 (w), 3049 (w), 2930 (w), 2860 (w), 1643 (m), 1525 (m), 1010 (s), 771 (s), 686 (s). ESI-MS: calculated: 391.1297, found: 390.1 ((*M*−H)$^-$, 90%), 269.1 (100%). HRMS: 392.1372 (*M*H$^+$, 100%).

*(E)-6-(4-(phenyldiazenyl)benzamido)hexyl dihydrogenphosphate (**4f**)*: Compound **3f** (24 mg, 0.074 mmol) was employed. Compound **4f** was obtained in 7% yield (1.9 mg, 0.005 mmol). HPLC: R_t = 14.0 min, 95% purity (220 nm), <99% purity (254 nm). ^{1}H NMR (400 MHz, CD_3OD): δ = 8.02–7.92 (m, 6H), 7.60–7.51 (m, 3H), 3.97 (q, J = 6.6 Hz, 2H), 3.41 (t, J = 7.1 Hz, 2H), 1.68 (dp, J = 13.7, 6.8 Hz, 4H), 1.46 (dd, J = 7.9, 4.4 Hz, 4H). ^{31}P NMR (162 MHz, CD_3OD): δ = 0.30. IR: $\tilde{\nu}$ = 3314 (w), 2930 (m), 2855 (m), 1625 (m), 1536 (m), 1014 (s), 775 (s). ESI-MS: calculated: 405.1454, found: 406.2 (*M*H$^+$, 25%), 274.3 (100%), 214.1 (90%); found: 404.1 ((*M*−H)$^-$, 100%). HRMS: 406.1526 (*M*H$^+$, 100%), 404.1388 ((*M*−H)$^-$, 100%).

Photophysical and photochemical characterization

UV/Vis absorption spectra of compounds **4a–f** were recorded with a JASCO V-650 spectrophotometer. Compound **4c** and the thermal lifetime of compound **4e** were analyzed with an Agilent 8453 spectrometer. For temperature control, a Varian Cary single-cell Peltier apparatus was used. The used solvent and concentration are stated for each experiment. UV-induced isomerization reactions were performed with a Soul Veasos single-spot LED (365 nm, 0.9 W), an OSRAM Oslon SSL 80 single-spot LED (455 nm, 1.2 W), or a Sylvania UV lamp with two 8 W fluorescent black-light bulbs (settings: 250 mA, 220 V). Sample volume was $\leq$1 mL. For direct photocontrol experiments, **4e** was isomerized by using a high-power LED (LED Engin, Osram; settings: 700 mA and 16 V) for 15 s. The sample volume was 200 μL.

Bacterial strains, plasmids, and chemicals

The proteins used in this work were produced in the *E. coli* expression strains *E. coli* BL21 Gold (DE3) (purchased from Agilent Technologies, Santa Clara, CA, USA) and *E. coli* BL21 (DE3) Rosetta (purchased from Novagen, Merck, Darmstadt, Germany). The following expression plasmids were taken from previously published work: pET28a TrpA, pET24a TrpB, and pET28a VioA.[24c] HRP was purchased from Sigma-Aldrich (St. Louis, MO, USA). IGP was produced enzymatically from 1-(*o*-carboxyphenylamino)-1-deoxyribulose-5-phosphate as described previously.[39] All other chemicals were purchased form commercial sources and were of analytical grade or higher.

Expression and purification of TS

The genes coding for TrpA and TrpB were heterologously expressed in BL21 (DE3) Rosetta and BL21 Gold (DE3), respectively. Cells containing expression vectors with the respective genes were grown at 37 °C to an OD_{600} of 0.6 in 2–6 L lysogeny broth (LB) medium supplemented with kanamycin. At this point, 0.5 mM isopropyl-β-D-thiogalactopyranosid (IPTG) was added to induce gene expression and cells were incubated overnight at 20 °C. The cells were harvested by centrifugation, resuspended in 100 mM potassium phosphate (KP) pH 7.5, 300 mM KCl, 20 mM imidazole (20 mL per 1 L cell suspension), and disrupted by sonication. Cell debris and insoluble aggregates were removed by centrifugation. Proteins were purified from the supernatant by nickel-affinity chromatography (HisTrap FF Crude column, 5 mL, GE Healthcare) with a linear gradient of imidazole (20 mM→500 mM) followed by size-exclusion chromatography (Superdex 75 HiLoad 26/600, GE Healthcare, Chicago, IL, USA) using 100 mM KP pH 7.5, 300 mM KCl as buffer. Fractions containing the purified protein were pooled and dripped into liquid nitrogen for storage at −80 °C.

Expression and purification of auxiliary enzymes

The auxiliary enzyme tryptophan oxidase (VioA) from *Chromobacterium violaceum* was expressed in BL21 Gold (DE3).[24c] Transformed *E. coli* strains were grown in 4L LB medium supplemented with kanamycin at 37 °C to an OD_{600} of 0.6. Then, protein expression was induced with 0.5 mM IPTG and cells were incubated overnight at 20 °C. Cells were harvested by centrifugation and the pellets were resuspended in 20 mM Tris·HCl pH 8.0, 300 mM NaCl, and 20 mM imidazole. The target protein was obtained from the supernatant after sonication and repeated centrifugation steps. VioA was captured by nickel-affinity chromatography (HisTrap FF Crude column, 5 mL, GE Healthcare, Chicago, IL, USA) and eluted with a linear gradient of imidazole (10→500 mM). Fractions containing the target protein were identified by SDS-PAGE analysis, pooled, and further purified by size-exclusion chromatography (Superdex 75 HiLoad 26/600, GE Healthcare, Chicago, IL, USA) with 20 mM Tris·HCl pH 8.0 as running buffer. Fractions containing the purified protein were pooled and dripped into liquid nitrogen for storage at −80 °C.

Steady-state activity measurements and inhibition studies

In general, steady-state enzyme kinetic measurements were performed at 25 °C and monitored spectrophotometrically by using a microplate reader (Infinite M200 Pro, TECAN, Männedorf, Switzerland). Turnover of IGP or indole to Trp was measured with a coupled enzymatic assay,[24c] employing VioA, which oxidized Trp to produce the side-product peroxide, and horseradish peroxidase (HRP), which then turned over peroxide with 4-aminoantipyrine and phenol to water and a quinone imine. Formation of the latter was monitored at 505 nm ($\Delta\varepsilon_{505}$ (quinone imine) = 6,400 M^{-1} cm^{-1}).[40] All reactions were started by addition of the TS complex in 1:1 stoichiometry. Reaction conditions were: 50 mM KP, pH 7.5, 100 mM KCl, 5 mM Ser, 1.0 mM phenol, 1 mM 4-aminoantipyrine, 20 μM pyridoxal phosphate (PLP), 0.15 g L^{-1} horseradish peroxidase (HRP), 1.0 g L^{-1} VioA, and varying concentrations of substrate (0–200 μM for indole, 0–150 μM for IGP). In order to determine turnover rates, the initial slopes v_i of the substrate turnover curves were measured and divided by the total enzyme concentration [E_t]. These turnover rates $v_i/[E_t]$ (in s^{-1}) were plotted against the substrate concentration [S]. Michaelis–Menten constants K_M and turnover numbers k_{cat} were determined by fitting the data with Equation (1)[28] by using Origin 2019 (OriginLab).

$$\frac{v_i}{[E_t]} = \frac{k_{cat}[S]}{K_M + [S]} \quad (1)$$

To identify the concentration range in which the azobenzenze-based compounds inhibited TS, activity measurements were performed with varying inhibitor concentrations and constant IGP and Ser concentrations. Reaction conditions were: 50 mM KP, pH 7.5, 100 mM KCl, 5 mM Ser, 1.0 mM phenol, 1.0 mM 4-aminoantipyrine, 20 μM PLP, 0.15 g L^{-1} HRP, 1.0 g L^{-1} VioA, 30 μM IGP, and 0–300 mM **4d–f**. Reactions were performed at 25 °C. After baseline detection, the reactions were started by addition of the 0.1 μM TS complex in 1:1 TrpA:TrpB stoichiometry. All measurements were performed by using a microplate reader (Infinite M200 Pro, TECAN, Männedorf, Switzerland). The initial reaction rates for different inhibitor concentrations were normalized to the reaction rate in the absence of inhibitor, and plotted against the logarithm of the inhibitor concentration.

To determine the mode of inhibition, steady-state kinetics were recorded for four different inhibitor concentrations, which corresponded to degrees of inhibition of 0% (0 mM), ≈30% (100 mM), ≈50% (175 mM), and ≈70% (250 mM), as measured in the previous setup. Reaction conditions were: 50 mM KP pH 7.5, 100 mM KCl, 5 mM L-serine, 1.0 mM phenol, 1.0 mM 4-aminoantipyrine, 20 μM PLP, 0.15 g L^{-1} HRP, 1.0 g L^{-1} VioA, and varying concentrations of substrate (0–150 μM for IGP and 0–200 μM for indole). Reactions were started by addition of 0.1 μM TS complex in 1:1 TrpA:TrpB stoichiometry. Fitting the data of a single kinetic experiment to the Michaelis–Menten equation [Eq. (1)] provided an apparent rate constant k_{cat}^{app} and the apparent Michaelis constant K_M^{app}. The values of the inhibition constant K_i and the α value, which describes the mode of inhibition, were determined by using a gener-

al model for enzyme inhibition.[28] For this, the steady-state kinetic data in presence of inhibitor was evaluated by plotting the measured reaction rates v_i divided by the total enzyme concentration [E_t] against the substrate concentration [S]. The values for k_{cat}, K_M, K_i, and α were determined by a global fit of the four inhibition curves for the four inhibitor concentrations [I] with Equation (2).[28]

$$\frac{v_i}{[E_t]} = \frac{k_{cat}[S]}{[S]\left(1+\frac{[I]}{\alpha K_i}\right)+K_M\left(1+\frac{[I]}{K_i}\right)} \quad (2)$$

Competitive inhibition is characterized by an infinite α value ($\alpha \rightarrow \infty$), because there is no binding of the inhibitor to the enzyme:-substrate (ES) complex. Uncompetitive inhibition leads to an α value close to zero ($\alpha \ll 1$), because there is no binding to the free enzyme.[28] In noncompetitive inhibition, there is affinity for both the ES complex and the free enzyme, which is characterized by a finite value of α.

Determination of binding constants

Binding constants were determined by means of ITC measurements with a MicroCal PEAQ-ITC system (Malvern). Solutions of protein (50–100 μM) and **4e** (1.0 mM) were prepared by using the same buffer stock (≈300 mM Tris·HCl, pH 8.0). Three control experiments, namely the titration of buffer with buffer, the titration of protein solution with buffer, and the titration of buffer with ligand, were performed. Each titration experiment was baseline corrected and the signal peaks of each injection were integrated by MicroCal PEAQ-ITC analysis (version 1.22, Malvern Panalytical). Then, each protein–ligand titration experiment was corrected for each control experiment and processed by using the built-in functions of MicroCal PEAQ-ITC analysis with the "single set of identical sites" option. Thus, a ΔH versus molar ratio (ligand:protein) plot and fit values for the binding constant K_D, the number of binding sites n, and the molar heat of ligand binding ΔH were obtained. The fitted number of binding sites in initial analyses was close to one. For better comparability, the number of binding sites was then set to one for all experiments.

Crystallization

Tryptophan synthase was cocrystallized with ligand **4e** by using the hanging-drop vapor-diffusion method. For this, TrpA and TrpB were complexed in equimolar amounts and supplemented with a twofold excess of ligand **4e** to final concentrations of 30 g L^{-1} TS complex and 750 μM ligand **4e** in 50 mM Tris·HCl pH 7.5. Then, 1 μL of the mixture was mixed with 1 μL of reservoir solution containing 7% PEG 8000 and 0.1 M sodium citrate, pH 5. Crystals grew within several weeks in a rod-like morphology. Crystals were mounted on a nylon loop and shock-frozen in liquid nitrogen without addition of further cryoprotectants.

Identification of tunnels with MOLE 2.5

To find cavities in the crystal structure of TS_{4e}, the graphical user interface of MOLE 2.5.17.4.24 was used. The structure of TS_{4e} was loaded into the program and tunnels were identified by applying the automated built-in protocol with default parameter settings, that is, a bottleneck radius of 1.25 Å, an origin radius of 5.00 Å, a surface cover radius of 10.00 Å, a bottleneck length of 0.00 Å, a cutoff ratio of 0.90, a minimum tunnel length of 0.00 Å, and a minimum pore length of 0.00 Å. The default weight function was the Voronoi scale. Note: we use the term "cavity" for the identified pocket, whereas Mole 2.5 uses the term "tunnel".

Docking with YASARA

Compound **4e** was docked to TrpB by VINA docking[41] as implemented in YASARA, by utilizing the YASARA2 force field.[33] For this, TrpB residues 85, 87, 109, 112, 114, 115, 166, 190, 350, 379, and 382 that surround the binding site were set as flexible. Compound **4e** was docked 100 times to different TrpB conformations and the results were sorted according to their estimated binding energies. Additionally, these poses were clustered into 17 distinct complex conformations that had a distance of at least 5 Å deduced as root mean square deviation of the heavy atoms of **4e**. Moreover, checking the planarity of the azobenzene moiety after each docking run confirmed that the integrity of the ligand was constantly preserved.

In situ irradiation

Reaction conditions for the direct photocontrol of enzymatic turnover included 50 mM KP pH 7.5, 100 mM KCl, 5 mM Ser, 1.0 g L^{-1} VioA, 0.075 g L^{-1} HRP, 100 μM IGP, 1.0 mM 4-aminoantipyrine, 1.0 mM phenol, 20 μM PLP, 200 μM **4e**, and 0.1 μM TS complex. The reaction was started by the addition of the 0.1 μM TS complex in 1:1 stoichiometry and monitored at $\lambda = 505$ nm with $\Delta\varepsilon_{505}$ (quinone imine) = 6400 $M^{-1}cm^{-1}$.[40] Measurements were performed in a plate reader (Tecan Infinite M200 Pro) and activities were deduced from the slopes of the transition curves. Altogether two samples and two controls were measured simultaneously. The reaction rate of the first sample was monitored in the dark. The second sample was irradiated during the initial linear-activity phase. Control experiments were performed either in the absence of **4e** or with buffer instead of TS complex. Irradiation of the second sample and the two controls was carried out by pausing the measurement in the plate reader, taking out the plate, and exposing the three wells to UV light, while keeping the other well (positioned furthest away), containing the first sample, covered. The samples were irradiated after 30 min for 15 s with 365 nm (Mouser, high-power LED, 365 nm, 1.7 V, 700 mA), which corresponded to the irradiation time necessary for $Z \rightarrow E$ isomerization under these conditions. The turnover curves of the irradiated second sample and control sample in the absence of **4e** were baseline-corrected by subtraction of the buffer control. The first sample was baseline corrected by subtraction of a linear fit of the first 20 min of the buffer control.

Acknowledgements

We thank Elisabeth Bauer, Sonja Fuchs, Jeannette Ueckert, and Sabine Laberer for excellent technical assistance, Stefanie Zwisele for preparing crystals of TS, and Karin Rustler for fruitful discussions. We are grateful to Dr. Stefano Crespi (University of Groningen) for his assistance regarding the PSD analysis. NAS thanks the Studienstiftung des Deutschen Volkes for a PhD scholarship. This work was supported by a grant of the Deutsche Forschungsgemeinschaft to RS (STE 891/12-2). Open access funding enabled and organized by Projekt DEAL.

Conflict of interest

The authors declare no conflict of interest.

Keywords: antibiotics · azo compounds · enzymes · inhibitors · photopharmacology

[1] a) M. Tyers, G. D. Wright, *Nat. Rev. Microbiol.* **2019**, *17*, 141 – 155; b) X. Didelot, K. B. Pouwels, *Nat. Med.* **2019**, *25*, 1033 – 1034.

[2] J. M. Stokes, K. Yang, K. Swanson, W. Jin, A. Cubillos-Ruiz, N. M. Donghia, C. R. MacNair, S. French, L. A. Carfrae, Z. Bloom-Ackermann, V. M. Tran, A. Chiappino-Pepe, A. H. Badran, I. W. Andrews, E. J. Chory, G. M. Church, E. D. Brown, T. S. Jaakkola, R. Barzilay, J. J. Collins, *Cell* **2020**, *180*, 688 – 702.e13.

[3] D. G. Brown, T. L. May-Dracka, M. M. Gagnon, R. Tommasi, *J. Med. Chem.* **2014**, *57*, 10144 – 10161.

[4] J. A. Shapiro, A. R. Kaplan, W. M. Wuest, *ChemBioChem* **2019**, *20*, 34 – 39.

[5] a) I. P. Crawford, *Bacteriol. Rev.* **1975**, *39*, 87 – 120; b) S. Raboni, S. Bettati, A. Mozzarelli, *Cell. Mol. Life Sci.* **2009**, *66*, 2391 – 2403.

[6] a) M. F. Dunn, *Arch. Biochem. Biophys.* **2012**, *519*, 154 – 166; b) C. C. Hyde, S. A. Ahmed, E. A. Padlan, E. W. Miles, D. R. Davies, *J. Biol. Chem.* **1988**, *263*, 17857 – 17871; c) M. Weyand, I. Schlichting, *Biochemistry* **1999**, *38*, 16469 – 16480.

[7] W. O. Weischet, K. Kirschner, *Eur. J. Biochem.* **1976**, *65*, 365 – 373.

[8] M. F. Dunn, V. Aguilar, P. Brzović, W. F. Drewe Jr, K. F. Houben, C. A. Leja, M. Roy, *Biochemistry* **1990**, *29*, 8598 – 8607.

[9] T. R. M. Barends, T. Domratcheva, V. Kulik, L. Blumenstein, D. Niks, M. F. Dunn, I. Schlichting, *ChemBioChem* **2008**, *9*, 1024 – 1028.

[10] a) P. S. Brzović, K. Ngo, M. F. Dunn, *Biochemistry* **1992**, *31*, 3831 – 3839; b) K. Kirschner, A. N. Lane, A. W. Strasser, *Biochemistry* **1991**, *30*, 472 – 478.

[11] K. S. Anderson, E. W. Miles, K. A. Johnson, *J. Biol. Chem.* **1991**, *266*, 8020 – 8033.

[12] a) S. Rhee, K. D. Parris, C. C. Hyde, S. A. Ahmed, E. W. Miles, D. R. Davies, *Biochemistry* **1997**, *36*, 7664 – 7680; b) T. R. Schneider, E. Gerhardt, M. Lee, P. H. Liang, K. S. Anderson, I. Schlichting, *Biochemistry* **1998**, *37*, 5394 – 5406.

[13] a) H. Ngo, N. Kimmich, R. Harris, D. Niks, L. Blumenstein, V. Kulik, T. R. Barends, I. Schlichting, M. F. Dunn, *Biochemistry* **2007**, *46*, 7740 – 7753; b) P. Pan, M. F. Dunn, *Biochemistry* **1996**, *35*, 5002 – 5013; c) M. F. Dunn, D. Niks, H. Ngo, T. R. M. Barends, I. Schlichting, *Trends Biochem. Sci.* **2008**, *33*, 254 – 264.

[14] a) M. Weyand, I. Schlichting, A. Marabotti, A. Mozzarelli, *J. Biol. Chem.* **2002**, *277*, 10647 – 10652; b) A. Marabotti, P. Cozzini, A. Mozzarelli, *Biochim. Biophys. Acta Protein Struct. Mol. Enzymol.* **2000**, *1476*, 287 – 299; c) A. Sachpatzidis, C. Dealwis, J. B. Lubetsky, P. H. Liang, K. S. Anderson, E. Lolis, *Biochemistry* **1999**, *38*, 12665 – 12674.

[15] K. A. Abrahams, J. A. G. Cox, K. Fütterer, J. Rullas, F. Ortega-Muro, N. J. Loman, P. J. Moynihan, E. Pérez-Herrán, E. Jiménez, J. Esquivias, D. Barros, L. Ballell, C. Alemparte, G. S. Besra, *Sci. Rep.* **2017**, *7*, 9430.

[16] S. Wellington, P. P. Nag, K. Michalska, S. E. Johnston, R. P. Jedrzejczak, V. K. Kaushik, A. E. Clatworthy, N. Siddiqi, P. McCarren, B. Bajrami, N. I. Maltseva, S. Combs, S. L. Fisher, A. Joachimiak, S. L. Schreiber, D. T. Hung, *Nat. Chem. Biol.* **2017**, *13*, 943 – 950.

[17] a) M. M. Lerch, M. J. Hansen, G. M. van Dam, W. Szymanski, B. L. Feringa, *Angew. Chem. Int. Ed.* **2016**, *55*, 10978 – 10999; *Angew. Chem.* **2016**, *128*, 11140 – 11163; b) K. Hüll, J. Morstein, D. Trauner, *Chem. Rev.* **2018**, *118*, 10710 – 10747; c) J. Morstein, D. Trauner, *Curr. Opin. Chem. Biol.* **2019**, *50*, 145 – 151.

[18] a) J. Luo, S. Samanta, M. Convertino, N. V. Dokholyan, A. Deiters, *ChemBioChem* **2018**, *19*, 2178 – 2185; b) N. L. Mutter, J. Volarić, W. Szymanski, B. L. Feringa, G. Maglia, *J. Am. Chem. Soc.* **2019**, *141*, 14356 – 14363; c) L. Nevola, M. Varese, A. Martín-Quirós, G. Mari, K. Eckelt, P. Gorostiza, E. Giralt, *ChemMedChem* **2019**, *14*, 100 – 106.

[19] a) G. M. Murawska, C. Poloni, N. A. Simeth, W. Szymanski, B. L. Feringa, *Chemistry* **2019**, *25*, 4965 – 4973; b) B. Heinrich, K. Bouazoune, M. Wojcik, U. Bakowsky, O. Vázquez, *Org. Biomol. Chem.* **2019**, *17*, 1827 – 1833.

[20] a) D. Bliman, J. R. Nilsson, P. Kettunen, J. Andréasson, M. Grøtli, *Sci. Rep.* **2015**, *5*, 13109; b) C. L. Fleming, P. A. Sandoz, T. Inghardt, B. Önfelt, M. Grøtli, J. Andréasson, *Angew. Chem. Int. Ed.* **2019**, *58*, 15000 – 15004; *Angew. Chem.* **2019**, *131*, 15142 – 15146; c) D. Kolarski, A. Sugiyama, G. Breton, C. Rakers, D. Ono, A. Schulte, F. Tama, K. Itami, W. Szymanski, T. Hirota, B. L. Feringa, *J. Am. Chem. Soc.* **2019**, *141*, 15784 – 15791; d) X. X. Zhou, L. Z. Fan, P. Li, K. Shen, M. Z. Lin, *Science* **2017**, *355*, 836 – 842; e) N. N. Mafy, K. Matsuo, S. Hiruma, R. Uehara, N. Tamaoki, *J. Am. Chem. Soc.* **2020**, *142*, 1763 – 1767.

[21] a) P. Pfaff, K. T. G. Samarasinghe, C. M. Crews, E. M. Carreira, *ACS Cent. Sci.* **2019**, *5*, 1682 – 1690; b) E. Teichmann, S. Hecht, *ACS Cent. Sci.* **2019**, *5*, 1645 – 1647.

[22] a) W. A. Velema, J. P. van der Berg, M. J. Hansen, W. Szymanski, A. J. M. Driessen, B. L. Feringa, *Nat. Chem.* **2013**, *5*, 924 – 928; b) M. Wegener, M. J. Hansen, A. J. M. Driessen, W. Szymanski, B. L. Feringa, *J. Am. Chem. Soc.* **2017**, *139*, 17979 – 17986.

[23] H. M. D. Bandara, S. C. Burdette, *Chem. Soc. Rev.* **2012**, *41*, 1809 – 1825.

[24] a) A. C. Kneuttinger, K. Straub, P. Bittner, N. A. Simeth, A. Bruckmann, F. Busch, C. Rajendran, E. Hupfeld, V. H. Wysocki, D. Horinek, B. König, R. Merkl, R. Sterner, *Cell Chem. Biol.* **2019**, *26*, 1501 – 1514.e9; b) A. C. Kneuttinger, M. Winter, N. A. Simeth, K. Heyn, R. Merkl, B. König, R. Sterner, *ChemBioChem* **2018**, *19*, 1750 – 1757; c) A. C. Kneuttinger, S. Zwisele, K. Straub, A. Bruckmann, F. Busch, T. Kinateder, B. Gaim, V. H. Wysocki, R. Merkl, R. Sterner, *Int. J. Mol. Sci.* **2019**, *20*, 5106.

[25] A. Fàbrega, J. Vila, *Clin. Microbiol. Rev.* **2013**, *26*, 308 – 341.

[26] J. Broichhagen, J. A. Frank, D. Trauner, *Acc. Chem. Res.* **2015**, *48*, 1947 – 1960.

[27] K. Rustler, P. Nitschke, S. Zahnbrecher, J. Zach, S. Crespi, B. König, *J. Org. Chem.* **2020**, *85*, 4079 – 4088.

[28] R. A. Copeland, *Enzymes: A practical Introduction to Structure, Mechanism, and Data Analysis*; Wiley-Interscience, Hoboken, **2000**.

[29] W. O. Weischet, K. Kirschner, *Eur. J. Biochem.* **1976**, *65*, 375 – 385.

[30] S. Rhee, K. D. Parris, S. A. Ahmed, E. W. Miles, D. R. Davies, *Biochemistry* **1996**, *35*, 4211 – 4221.

[31] a) A. R. Buller, P. van Roye, J. K. B. Cahn, R. A. Scheele, M. Herger, F. H. Arnold, *J. Am. Chem. Soc.* **2018**, *140*, 7256 – 7266; b) M. Herger, P. van Roye, D. K. Romney, S. Brinkmann-Chen, A. R. Buller, F. H. Arnold, *J. Am. Chem. Soc.* **2016**, *138*, 8388 – 8391.

[32] D. Sehnal, R. Svobodová Vařeková, K. Berka, L. Pravda, V. Navrátilová, P. Banáš, C.-M. Ionescu, M. Otyepka, J. Koča, *J. Cheminf.* **2013**, *5*, 39.

[33] E. Krieger, G. Vriend, *Bioinformatics* **2014**, *30*, 2981 – 2982.

[34] W. A. Velema, M. J. Hansen, M. M. Lerch, A. J. M. Driessen, W. Szymanski, B. L. Feringa, *Bioconjugate Chem.* **2015**, *26*, 2592 – 2597.

[35] a) D. Bléger, J. Schwarz, A. M. Brouwer, S. Hecht, *J. Am. Chem. Soc.* **2012**, *134*, 20597 – 20600; b) S. Samanta, A. A. Beharry, O. Sadovski, T. M. McCormick, A. Babalhavaeji, V. Tropepe, G. A. Woolley, *J. Am. Chem. Soc.* **2013**, *135*, 9777 – 9784.

[36] a) J. Calbo, C. E. Weston, A. J. P. White, H. S. Rzepa, J. Contreras-García, M. J. Fuchter, *J. Am. Chem. Soc.* **2017**, *139*, 1261 – 1274; b) S. Crespi, N. A. Simeth, B. König, *Nat. Rev. Chem.* **2019**, *3*, 133 – 146.

[37] a) D. G. J. Larsson, A. Andremont, J. Bengtsson-Palme, K. K. Brandt, A. M. de Roda Husman, P. Fagerstedt, J. Fick, C.-F. Flach, W. H. Gaze, M. Kuroda, K. Kvint, R. Laxminarayan, C. M. Manaia, K. M. Nielsen, L. Plant, M.-C. Ploy, C. Segovia, P. Simonet, K. Smalla, J. Snape, E. Topp, A. J. van Hengel, D. W. Verner-Jeffreys, M. P. J. Virta, E. M. Wellington, A.-S. Wernersson, *Environ. Int.* **2018**, *117*, 132 – 138; b) K. Kummerer, *J. Antimicrob. Chemother.* **2004**, *54*, 311 – 320.

[38] a) P. Lentes, E. Stadler, F. Röhricht, A. Brahms, J. Gröbner, F. D. Sönnichsen, G. Gescheidt, R. Herges, *J. Am. Chem. Soc.* **2019**, *141*, 13592 – 13600; b) J. B. Trads, K. Hüll, B. S. Matsuura, L. Laprell, T. Fehrentz, N. Görldt, K. A. Kozek, C. D. Weaver, N. Klöcker, D. M. Barber, D. Trauner, *Angew. Chem. Int. Ed.* **2019**, *58*, 15421 – 15428; *Angew. Chem.* **2019**, *131*, 15567 – 15574.

[39] S. Schlee, S. Dietrich, T. Kurćon, P. Delaney, N. M. Goodey, R. Sterner, *Biochemistry* **2013**, *52*, 132 – 142.

[40] M. J. Green, H. A. O. Hill, *Methods Enzymol.* **1984**, *105*, 3 – 22.

[41] O. Trott, A. J. Olson, *J. Comput. Chem.* **2010**, *31*, 455 – 461.

Manuscript received: September 7, 2020
Revised manuscript received: October 16, 2020
Accepted manuscript online: October 20, 2020
Version of record online: December 22, 2020

